Durham University

Durham E-Theses

Diffusion Equilibrium Times for Langmuir Isotherm Adsorption in Shale and Coalbed Methane Systems

CATHERINE ROBINIA HODSON

How to cite:

HODSON, CATHERINE ROBINIA (2019) Diffusion Equilibrium Times for Langmuir Isotherm Adsorption in Shale and Coalbed Methane Systems. Masters thesis, Durham University.

Use policy

The full-text may be used and/or reproduced, and given to third parties in any format or medium, without prior permission or charge, for personal research or study, educational, or not-for-profit purposes provided that:

- a full bibliographic reference is made to the original source
- a https://etheses.durham.ac.uk/id/eprint/13088/ is made to the metadata record in Durham E-Theses
- the full-text is not changed in any way

The full-text must not be sold in any format or medium without the formal permission of the copyright holders.

Please consult the full Durham E-Theses policy for further details.

Academic Support Office, The Palatine Centre, Durham University, Stockton Road, Durham, DH1 3LE
e-mail: e-theses.admin@durham.ac.uk Tel: +44 0191 334 6107
https://etheses.durham.ac.uk

Diffusion Equilibrium Times for Langmuir Isotherm Adsorption in Shale and Coalbed Methane Systems

Catherine Hodson

A thesis submitted for the degree of Master of Science
at Durham University

Department of Earth Sciences
Durham University

October 2018

Abstract

The 'quasi-steady state' (QSS) assumption is a commonly applied simplification to numerical dual porosity models. However, the assumption only becomes valid when concentration changes within the fractures are slow in relation to the time required for diffusive equilibrium to occur within the matrix (Barker, 1991).

This thesis seeks to explore diffusion equilibrium times (DET) for gas diffusion with Langmuir isotherm adsorption by numerical solution and sensitivity analysis. A simple, heuristic function is derived, permitting rapid estimation of DET for individual cases. Four short case studies exploring application to shale gas and coalbed methane systems are presented.

Contents

Abstract **1**

List of Figures **4**

List of Tables **5**

Nomenclature **6**

Declaration **8**

1 Introduction **9**

1.1 Research objective 10

1.2 Thesis overview 11

2 Key Concepts in Shale and Coal **12**

2.1 Gas storage 12

2.2 Gas transport 13

2.2.1 Fracture flow processes 13

2.2.2 Matrix flow processes 13

2.3 Sorption 15

3 Mathematical Models **18**

3.1 Diffusive representation 18

3.2 Quasi-steady state representation 19

3.3 Dimensionless transformation 20

3.4 Numerical solution 22

3.5 Determination of a diffusion equilibrium time 23

4 Results & Discussion **24**

4.1 Results 24

4.1.1 Application to shale gas systems 26

4.1.2 Application to coalbed methane systems 27

5 Conclusions & Recommendations **29**

5.1 Conclusions 29

5.2 Recommendations for further work 30

References **39**

A Case study parameters - shale **40**

B Case study parameters - coal **41**

List of Figures

4.1 Plots of dimensionless diffusive flux, J_{0D}, against dimensionless time, τ, for a range of $\beta = 1000$ and γ scenarios. 25

4.2 Plots of absolute dimensionless error between the diffusive fluxes calculated using the diffusive model and the quasi-steady-state model. 26

4.3 Evaluated dimensionless diffusion equilibrium times, τ_{cr}, against γ for various β scenarios. 27

List of Tables

4.1 Calculated diffusion equilibrium times - shale cases 27

4.2 Calculated diffusion equilibrium times - coalbed methane cases 28

A.1 Study parameters - shale cases 40

B.1 Study parameters - coalbed methane cases 41

Nomenclature

		First used in
Roman Symbols		
a	Empirical constant	Eq. (3.1), p.18
b	Empirical constant	Eq. (3.1), p.18
C	Adsorbed species concentration	Eq. (2.4), p.15
c	Mass concentration of gas in matrix porosity	Eq. (3.1), p.18
D	Diffusion coefficient	Eq. (3.2), p.19
d	Diameter	Eq. (2.3), p.14
E	Normalised absolute error	Eq. (3.22), p.23
g	Acceleration due to gravity	Eq. (2.1), p.13
J	Diffusive flux	Eq. (3.4), p.19
k	Permeability	Eq. (2.1), p.13
L	Thickness of matrix slab	Eq. (3.3), p.19
M	Molecular mass	Eq. (2.3), p.14
n	System geometry factor	Eq. (3.18), p.22
P	Pressure	Eq. (2.1), p.13
q	Darcy flux	Eq. (2.1), p.13
R	Universal gas constant	Eq. (2.3), p.14
s	Mass of sorbed gas per unit mass rock matrix	Eq. (3.1), p.18
T	Temperature	Eq. (2.3), p.14
t	Time	Eq. (3.2), p.19
x	Distance from and normal to fracture surface	Eq. (3.2), p.19
Greek Symbols		
α	Empirical mass transfer coefficient	Eq. (3.5), p.19
β	Dimensionless parameter	Eq. (3.10), p.20
δ	Pore constrictivity	Eq. (2.2), p.14
γ	Dimensionless parameter	Eq. (3.10), p.20
μ	Dynamic viscosity	Eq. (2.1), p.13

ϕ	Porosity	Eq. (3.2), p.19
ρ	Density	Eq. (3.2), p.19
τ	Dimensionless time	Eq. (3.10), p.20
υ	Tortuosity	Eq. (2.2), p.14
ξ	Dimensionless distance	Eq. (3.10), p.20
ζ	Chemical potential	Eq. (2.4), p.15

Subscripts

0	Fracture	Eq. (3.3), p.19
b	Bulk	Eq. (3.2), p.19
cr	Critical, diffusion equilibrium	Eq. (3.23), p.23
D	Dimensionless	Eq. (3.11), p.21
E	Effective	Eq. (3.2), p.19
I	Initial	Eq. (3.3), p.19
i	Gas species identifier	Eq. (2.3), p.14
j	Phase identifier	Eq. (2.1), p.13
K	Knudsen	Eq. (2.3), p.14
m	Matrix	Eq. (3.5), p.19
p	Pore	Eq. (2.3), p.14
r	Relative	Eq. (2.1), p.13
s	Sorbed	Eq. (2.4), p.15
s0	Surface at zero loading	Eq. (2.4), p.15
surf	Surface	Eq. (2.4), p.15

Superscripts

*	Quasi-steady state	Eq. (3.7), p.20

Declaration

I declare that this thesis, presented for the degree of Master of Science at Durham University, is a result of my own original research and has not been previously submitted to Durham University or any other institution. I have clearly indicated, when appropriate, the contributions of colleagues and have made every effort to acknowledge all collaborative work.

The copyright to the material within this thesis belongs to the author and any information or quotation taken from it, should be acknowledged and published only if prior consent has been given.

Catherine Hodson
Durham University
July 2018

Chapter 1

Introduction

Much recent work has sought to develop understanding of gas production from unconventional shale and coalbed methane reservoirs. In the US, shale gas production continues to expand, with total production volumes increasing by close to 50% between 2013 and 2016 and accounting for 62% of domestic natural gas production in 2016 (U.S.E.I.A, 2018). While US production from coalbed methane recently declined by 20% between 2015 and 2016 and is less significant than shale, considerable reserves remain (U.S.E.I.A, 2018).

Shale and coal are examples of fractured porous media. Flow in such media is often studied with numerical dual porosity models. These models assume that the storage capacity of the porous matrix is much greater than that of the fractures, while the permeability of the fractures is significantly higher than that of the matrix. Furthermore, it is assumed that flow within the matrix, parallel to fractures is negligible (Barenblatt et al., 1960).

However, reservoirs such as shale and coal may be described as special cases of dual porosity media (Bello and Wattenbarger, 2010), since these reservoirs contain a high proportion of adsorbed gas in contrast to the volumes stored in open pore space in more conventional reservoirs. In addition, the small scale of porosity in shale and coal means that diffusion processes dominate flow within the matrix.

Dual porosity models may take distinct approaches to the representation of fracture-

matrix exchange.

Diffusive models employ Fick's Second Law to describe the diffusive flux within the matrix block and at the matrix-fracture boundary.

Contrastingly, Quasi-steady State (QSS) models characterise the matrix block using a single potential. The matrix-fracture flux is then assumed to be proportional to the difference in potentials between the two porosities. Importantly, QSS models assume that quasi-steady flow conditions are present from the beginning of flow.

QSS models are appealing, since they are computationally efficient in comparison to fully diffusive models. However, application of QSS models to shale gas and coalbed methane production may be questionable for two main reasons.

Firstly, the QSS approach adopts the assumption that, at any given time, the pressure in the matrix is decreasing at the same rate throughout. Usually, such a pressure distribution would take a significant time to develop and in low permeability formations, the time to achieve this state may be extended.

Secondly, the inclusion of Langmuir isotherm adsorption within the matrix introduces a non-linearity that may further influence the time taken for a QSS model to adequately represent the system.

A study is required to examine the effect of Langmuir isotherm adsorption on time taken to achieve 'diffusive equilibrium', at which point QSS conditions may be assumed.

Understanding the time to achieve diffusive equilibrium permits appropriate application of the QSS assumption, with the associated benefits of computational efficiency. It also highlights situations where further investigation may be required or where a more suitable representation, such as a fully diffusive model, must be employed.

1.1 Research objective

This study seeks to explore diffusion equilibrium times (DETs) for gas diffusion with Langmuir isotherm adsorption by numerical solution and sensitivity analysis. A heuristic function permitting rapid estimation of DET for individual cases is sought.

1.2 Thesis overview

Understanding gas storage, transport and the significance of adsorption is central to effective production modelling of shale and coal reservoirs. It is noted that considerable uncertainty often exists in relation to the key properties of individual reservoirs. The following chapter highlights key concepts and approaches to modelling reservoir storage, flow and sorptive processes, informing the development of an appropriate mathematical model.

In Chapter 3, a diffusive representation of the gas sorptive system is derived, incorporating Langmuir isotherm adsorption. A quasi-steady state (QSS) approximation to the diffusive problem is then made and both models are subject to dimensionless transformation. The procedure for numerical solution is described, along with the process for determination of DET.

In Chapter 4, model scenarios are plotted and discussed in relation to the dimensionless parameter groups identified in the previous chapter. A simple, heuristic function is found to approximate a significant part of the analysis. Four short case studies explore the models' application to shale and coalbed methane systems.

The thesis closes in Chapter 5, with summary concluding remarks and recommendations for further work.

Chapter 2

Key Concepts in Shale and Coal

2.1 Gas storage

In shale and coal, gas may be stored as free gas in natural fractures and voids, adsorbed on organic and inorganic surfaces or dissolved in oil or water (Curtis, 2002; Zhang et al., 2012; Shi and Durucan, 2008).

Coal is characterised by a relatively uniform network of natural fractures or 'cleats', with spacing on the order of millimetres to centimetres, with blocks of porous matrix between the cleats. The porosity of coal matrix is heterogeneous, with pore size varying from the Angstrom to the micrometre scale (Shi and Durucan, 2008).

A shale matrix, however, is typically of low, anisotropic permeability, with permeabilities in the range of 10-100 nD (Cipolla et al., 2010; Yang and Aplin, 2007). Naturally occurring fractures are likely to be present but the relatively uniform fracture network found in coal is not typically seen. Mineralogy and a high degree of compositional heterogeneity influence pore size distribution, transport and gas flow properties and response to stimulation treatments (Curtis et al., 2012; Rickman et al., 2008; Sondergeld et al., 2010; Kuila and Prasad, 2011).

In shale, matrix porosity has been found to consist of intra-particle, inter-particle and organic matter intra-particle pores. Pore sizes vary from the order of 3-100 nm for intra-particle pores up to micrometres for inter-particle pores (Loucks et al., 2012;

Curtis et al., 2011). Organic matter porosity is distinct, since such pores are relatively poorly connected and the fraction of gas in the sorbed phase is comparable to that of the free gas in the open pore space (Loucks et al., 2012).

2.2 Gas transport

In fractured, porous media, it is important to note the distinct flow processes occurring in the fractures, relative to those in the relatively low-permeability porous matrix. This section identifies the processes relevant to the cases of shale and coal.

2.2.1 Fracture flow processes

Gas flow in fractures is usually taken to be adequately represented by laminar, Darcy flow (Shi and Durucan, 2008; Moridis et al., 2010). Single phase flow is generally accepted in shale, since minimal water is generally produced (Sondergeld et al., 2010). In CBM, however, initial production involves dewatering the coal. Over time, two phase flow develops and only at later times may gas production be adequately represented by single phase flow (Shi and Durucan, 2008).

The multiphase form of Darcy's law is given by Eq. (2.1)

$$\mathbf{q_j} = -\frac{\mathbf{k}\mathbf{k_{rj}}}{\mu_\mathbf{j}} \left(\nabla \mathbf{P_j} + \rho_\mathbf{j} \mathbf{g}\right) \tag{2.1}$$

2.2.2 Matrix flow processes

In the low-permeability matrix, diffusion is the dominant transport process (Shi and Durucan, 2008). Diffusion in shale and coal is a combination of three distinct processes, namely molecular diffusion, Knudsen diffusion and surface diffusion (Dong et al., 2017).

Molecular diffusion occurs where collisions between molecules dominate and is generally prevalent where the pore diameter is greater than ten times the mean free path (Yang, 1997). The diffusive flux is proportional to the concentration gradient

of the diffusing species. In porous media, the effective diffusion coefficient, D_E [L^2 T^{-1}], may be estimated from the true diffusion coefficient, D [L^2 T^{-1}], by considering the effective porosity available for flow, ϕ_E [-], pore constrictivity, δ [-], and pore tortuosity, υ [-], as in Eq. (2.2).

$$D_E = \frac{D\phi_E\delta}{\upsilon} \tag{2.2}$$

Where pore diameters are smaller or the diffusing gas is at low pressure, a transition to the dominance of molecule-wall collisions occurs, leading to development of Knudsen diffusion. The molecule-wall collisions have the effect of reducing gas flux relative to molecular diffusion. The Knudsen diffusivity, D_{iK}, of a gas species, i, can be estimated with Eq. (2.3)

$$D_{iK} = \frac{d_p}{3}\sqrt{\frac{8RT}{\pi M_{ri}}} \tag{2.3}$$

where d_p [L] is the mean pore diameter of the porous medium, M_{ri} is the molecular weight of gas species i, R is the Universal Gas Constant and T is temperature.

The mean free path of methane at room temperature and atmospheric pressure (0.1 MPa) has been estimated at 50 nm (Thimmons and Kissell, 1973). Given the typical *in situ* conditions of CBM and shale gas reservoirs, molecular and transition diffusion would be expected to dominate (Shi and Durucan, 2008; Sondergeld et al., 2010; Xu et al., 2015). Knudsen diffusion may only contribute significantly at late times where low pressure occurs in a reservoir.

However, in very small pores, Dubinin's theory of micropore volume filling combined with Polanyi's adsorption potential theory leads to an additional theory of diffusion. In small pores, gas molecules are always subject to van der Waals forces due to the proximity of the pore walls. Thus, diffusing molecules are always within the potential field of the adsorbing surface and behave more as a liquid. Diffusion occurs through an activated process whereby molecules 'jump' between sites of sorption (Shi and Durucan,

2008). This process may be regarded as similar to a surface diffusion process, driven by gradients in the chemical potential of adsorbed species.

The surface diffusivity, D_{surf}, may be represented as in Eq. (2.4)

$$D_{surf} = D_{s0} \frac{1}{RT} \frac{\partial \zeta_s}{\partial \ln C_s} \tag{2.4}$$

where D_{s0} is the surface diffusivity at zero loading, ζ_s is the chemical potential of the adsorbed species and C_s is the concentration of the sorbed species. Thus, we note that surface diffusion is a more complex process than molecular or Knudsen diffusion, since D_s, is dependent on both the diffusing particles and the substrate. Further, lateral interactions between diffusing particles must be accounted for leading to a strong dependence of surface diffusivity on surface coverage (Medved and Cerny, 2011).

2.3 Sorption

Sorption is an important consideration in both shale gas and CBM production. Between 20 and 85% of gas in shale is reported to be present in the sorbed state (Hill and Nelson, 2000). Similarly, in the CBM environment, the primary storage mechanism is understood to be sorption, accounting for up to 98% of storage (Shi and Durucan, 2008). Thus, the inclusion of sorption may be fundamental to the appropriate characterisation of fracture-matrix exchange.

Desorption has been found to be particularly significant to gas production at later times when quasi-steady state flow is established (Gao et al., 1994; Shi and Durucan, 2008; Moridis et al., 2010; Cheng, 2011). In a study by Cheng (2011), the inclusion of desorption led to 20% more gas volume production compared to the case of no desorption over a 50-year run-time, due to a higher late-time gas rate. Similarly, Cipolla et al. (2010) found that most of the additional production due to desorption occurs later in a well's life. Su et al. (2015) found that a larger Langmuir volume is associated with longer-lasting, early-time, transient flow and therefore, longer lasting higher rates of

production. Larger sorbed gas volumes have been found to delay fracture interference in multiply-fractured wells, thereby postponing the production rate decline associated with fracture interference (Freeman et al., 2013).

Sorption studies have often demonstrated the adequacy of the Langmuir isotherm for modelling methane desorption in shale and clay (Bumb and McKee, 1988; Gao et al., 1994; Shi and Durucan, 2008; Hu, 2014).

The Langmuir isotherm model assumes that equilibrium between the sorptive surface and free gas in the pore space occurs instantaneously in response to a change in gas pressure. Since shale is of very low permeability and flow through the matrix is very slow, the instantaneous equilibrium assumption may be considered as valid (Gao et al., 1994; Freeman et al., 2013). The Langmuir model assumes that the sorbed phase forms a monolayer (sorbed layer is one molecule in thickness). Sorption can occur only at a fixed number of sites that are identical and equivalent. There is assumed to be no interaction or steric hindrance between sorbed molecules. All sorption sites possess equal affinity for the sorbate and the sorbate does not migrate across the surface of the sorbent (Foo and Hameed, 2010).

Equilibrium constants for the process of gas sorption in coal and shale will be temperature dependent. However, isothermal modelling in shale is considered appropriate (Moridis et al., 2010) and the isothermal assumption facilitates computation of the real properties of methane from an appropriate equation of state (Freeman et al., 2013).

The gas sorption capacity of coal and shale is typically influenced by pressure, temperature, moisture content, organic material composition and mineral content (Crosdale et al., 1998; Hildenbrand et al., 2006; Krooss et al., 2002).

In certain circumstances, alternative sorption modelling approaches may be advocated (Shi and Durucan, 2008; Leahy-Dios et al., 2011; Ambrose et al., 2011). For instance, a recent evaluation of adsorption models for methane in shales found that a dual-site Langmuir model was the only model to fit the data well, interpret all observed test phenomena and predict test data beyond measurements (Tang et al., 2017). Alter-

natively, where a pore-filling adsorption process is present, a related model such as the Dubinin-Raduskevich model may be applied.

Further issues related to sorption in nanoporous media include the potential effects of ad/desorption on matrix porosity and permeability (Ambrose et al., 2010; Sinha et al., 2013). Additionally, the relatively low pressures required for desorption should be considered in conjunction with stress-dependent permeability to more fully understand the contribution of sorbed gas to production (Ambrose et al., 2010). Stress-dependent permeability may be less important in reservoirs with high Young's modulus values (Cipolla et al., 2010). Permeability change in shales as a function of reservoir pressure may result from ad/desorption, pore shrinkage due to depletion or Knudsen flow effects, where gas slippage alters the apparent gas permeability (Freeman et al., 2013; Ding et al., 2014; Sakhaee-Pour and Bryant, 2011; Allan and Mavko, 2013). Allan and Mavko (2013) investigated the effects of sorption and Knudsen diffusion on microporous rocks at pressures between atmoshperic (0.101 MPa) and 40 MPa. They found that adsorption could reduce permeability by up to 40% at high pressures and Knudsen diffusion increases permeability at lower pressures (by up to five times at 1 MPa).

Interestingly, Pillalamarry et al. (2011) also notes a bimodal trend in the variation of diffusion coefficient with pressure in coal. At high pressures, the diffusion coefficient remains relatively constant. However, as pressure is decreased, at a certain point the diffusion coefficient begins to increase almost exponentially. They suggest that desorption is responsible for the increase in diffusion coefficient and note that this could significantly influence production predictions from coal at low reservoir pressures (late-time production).

The non-linearity associated with sorption challenges its inclusion in analytical solutions (Freeman et al., 2013). It also requires that where a QSS model is considered for coal or shale that the applicability of the model is demonstrated, since the non-linearity may render the QSS approximation unsuitable.

Chapter 3

Mathematical Models

Having established the significance of adsorption to gas production from shale and coal in Chapter 2, Section 3.1 now develops a mathematical model that permits diffusion and Langmuir isotherm desorption within the rock matrix. A quasi-steady state approximation to this model is then developed in Section 3.2. Both models then undergo dimensionless transformation and dimensionless parameter groups are identified to aid understanding of the system. The procedure for numerical solution is described in Section 3.4 and the Diffusion Equilibrium Time is defined in Section 3.5.

3.1 Diffusive representation

Consider a set of parallel planar fractures separated by slabs of rock matrix of thickness L [L], porosity, ϕ [-], and bulk density, ρ_b [ML^{-3}]. Let c [ML^{-3}] be the mass concentration of gas in the pore-space of the rock matrix. The gas is assumed to adsorb to the rock grains according to the Langmuir sorption isotherm:

$$s = \frac{bc}{1 + ac} \tag{3.1}$$

where s [-] is the mass of adsorbed gas per unit mass of rock matrix and a [M^{-1}L^3] and b [M^{-1}L^3] are empirical constants describing the adsorption process.

One-dimensional diffusion of the gas within the rock matrix from a given fracture surface is described by

$$\phi\frac{\partial c}{\partial t}+\rho_b\frac{\partial s}{\partial t}=\left[\phi+\frac{\rho_b b}{(1+ac)^2}\right]\frac{\partial c}{\partial t}=D_E\frac{\partial^2 c}{\partial x^2} \tag{3.2}$$

where t [T] is time, D_E [L^2T^{-1}] is the effective diffusion coefficient of the gas and x [L] is distance from and normal to a nearby fracture surface.

A relevant set of initial and boundary conditions are as follows:

$$\begin{aligned} &c=c_I, && 0\le x\le L/2, && t=0\\ &c=c_0, && x=0, && t>0\\ &\partial c/\partial x=0, && x=L/2, && t>0 \end{aligned} \tag{3.3}$$

where c_I [ML^{-3}] represents a uniform initial mass concentration of the gas within the rock matrix and c_0 [ML^{-3}] represents a constant mass concentration of gas within the fractures.

Of particular interest is the diffusive flux of the gas from the rock matrix into the fractures, defined by

$$J_0=D_E\left.\frac{\partial c}{\partial x}\right|_{x=0}=-\int_0^{L/2}\left(\phi\frac{\partial c}{\partial t}+\rho_b\frac{\partial s}{\partial t}\right)dx \tag{3.4}$$

3.2 Quasi-steady state representation

In many cases, it is commonly assumed that the diffusive problem described previously can be well approximated by the following simplified, quasi-steady state (QSS), problem

$$\left[\phi+\frac{\rho_b b}{(1+ac_m)^2}\right]\frac{\partial c_m}{\partial t}=\alpha(c_0-c_m) \tag{3.5}$$

where α [T^{-1}] is an empirical mass transfer coefficient and c_m represents the mean c value within the rock matric, as defined by:

$$c_m = \frac{2}{L}\int_0^{L/2} c dx \tag{3.6}$$

from which it follows, considering Eq. (3.4), that

$$J_0^* = \frac{\alpha L}{2}(c_m - c_0) \tag{3.7}$$

The star superscript in Eq. (3.7) is hereafter used to indicate that QSS conditions are assumed.

The relevant initial condition in this case is:

$$c_m = c_I, \quad t = 0 \tag{3.8}$$

By studying the large time asymptotic behavior of the diffusive model described in Section 3.1, Mathias and Zimmerman (2003) show that, for scenarios where $a = 0$, the QSS model will match the diffusive model at large times if α is defined by

$$\alpha = \frac{\pi^2 D_E}{L^2} \tag{3.9}$$

3.3 Dimensionless transformation

For scenarios where $a > 0$, the mathematical problem must be solved numerically. To gain insight from a set of numerical simulations in this respect it is helpful to apply the following dimensionless transformations:

$$\xi = \frac{2x}{L}, \quad \tau = \frac{4D_E t}{\phi L^2}, \quad \beta = \frac{\rho_b b}{\phi}, \quad \gamma = a c_I \tag{3.10}$$

$$c_D = \frac{c}{c_I}, \quad c_{mD} = \frac{c_m}{c_I}, \quad c_{0D} = \frac{c_0}{c_I}, \quad J_{0D} = \frac{LJ_0}{2D_E c_I} \tag{3.11}$$

such that the diffusive problem, described in Section 3.1, reduces to:

$$\left[1 + \frac{\beta}{(1+\gamma c_D)^2}\right] \frac{\partial c_D}{\partial \tau} = \frac{\partial^2 c_D}{\partial \xi^2} \tag{3.12}$$

$$\begin{aligned} &c_D = 1, && 0 \le \xi \le 1, && \tau = 0 \\ &c_D = c_{0D}, && \xi = 0, && \tau > 0 \\ &\partial c_D / \partial \xi = 0, && \xi = 1, && \tau > 0 \end{aligned} \tag{3.13}$$

$$J_{0D} = \left.\frac{\partial c_D}{\partial \xi}\right|_{\xi=0} \tag{3.14}$$

and the QSS problem, described in Section 3.2, reduces to (assuming α is defined by Eq. (3.9)):

$$\left[1 + \frac{\beta}{(1+\gamma c_{mD})^2}\right] \frac{\partial c_{mD}}{\partial \tau} = \frac{\pi^2}{4}(c_{0D} - c_{mD}) \tag{3.15}$$

$$J^*_{0D} = \frac{\pi^2}{4}(c_{mD} - c_{0D}) \tag{3.16}$$

$$c_{mD} = c_{ID}, \quad \tau = 0 \tag{3.17}$$

Our main focus concerns gas production from shale or coal. In this context, it is relevant to fix $c_{0D} = 0$, which represents an extreme scenario whereby gas is immediately removed from fractures on arrival from the rock matrix. It can now be understood that there are just two parameters of concern: β and γ. The β parameter represents the ratio of adsorbed gas mass to free-phase gas mass within the rock matrix as the rock approaches depletion. The γ parameter indicates how initially close the rock matrix is to gas saturation (where all the sorption sites are occupied). If the rock matrix is initially gas saturated, $\gamma = 1$. If the rock matrix is initially under-saturated,

$0 \leq \gamma < 1$. Interestingly, the case when $\gamma \to \infty$ corresponds to a situation when there is no adsorption.

Considering the analytical solutions previously presented by Mathias and Zimmerman (2003), it can be understood that:

$$\lim_{\gamma \to 0} J_{0D} = 2 \sum_{n=0}^{\infty} \exp \left[-\frac{\pi^2}{4} \frac{(2n+1)^2 \tau}{(1+\beta)} \right] \tag{3.18}$$

$$\lim_{\gamma \to \infty} J_{0D} = 2 \sum_{n=0}^{\infty} \exp \left[-\frac{\pi^2}{4} (2n+1)^2 \tau \right] \tag{3.19}$$

$$\lim_{\gamma \to 0} J^*_{0D} = \frac{\pi^2}{4} \exp \left[-\frac{\pi^2}{4} \frac{\tau}{(1+\beta)} \right] \tag{3.20}$$

$$\lim_{\gamma \to \infty} J^*_{0D} = \frac{\pi^2}{4} \exp \left[-\frac{\pi^2}{4} \tau \right] \tag{3.21}$$

3.4 Numerical solution

Eqs. (3.12) to (3.14) were solved numerically using a similar methodology as described by Mathias et al. (2008). To summarise, the partial differential equation in Eq. (3.12) was discretised in space using finite differences. The resulting set of non-linear ordinary differential equations (ODE) with respect to time was then integrated collectively using MATLAB's stiff ODE solver, ODE15s. The dimensionless distance, ξ, was discretised into 100 logarithmically spaced points, with space steps ranging across three orders of magnitude. Manual specification of a time-step was not required because ODE15s adaptively chooses time-steps as the solution progresses. The numerical solutions were verified by setting $\gamma = 0$ and comparing results with those from Eq. (3.18).

Eqs. (3.15) to (3.17) were also solved numerically using MATLAB's stiff ODE solver, ODE15s.

3.5 Determination of a diffusion equilibrium time

A normalised measure of absolute error between the diffusive and QSS models, E [-], is hereafter defined as

$$E = |J_{0D} - J^*_{0D}| \tag{3.22}$$

For straightforward diffusion problems (i.e., when $a = 0$), the diffusion equilibrium time, t_{cr} [T], for the problem described in Section 3.1 is widely understood to be found from $t_{cr} = \phi L^2/(4D_E)$, which corresponds to a value of $\tau = 1$. In this study, when $a = 0$, $t_0 = (\phi + \rho_b b)L^2/(4D_E)$, which corresponds to a value of $\tau = 1 + \beta$.

Note that when $b = 0$, a value of E can be determined from Eqs. (3.19) and (3.21). The value of E when $\tau = 1$, using Eqs. (3.19) and (3.21) is 0.03964.

At this stage it is useful to define a dimensionless diffusion equilibrium time, τ_{cr}, using the expression

$$\tau_{cr} = \frac{4D_E t_{cr}}{\phi L^2} \tag{3.23}$$

Equivalent values of τ_{cr} for non-zero combinations of α and β can be evaluated by determining the final τ value at which $E = 0.03964$ using the numerical solutions described above.

Chapter 4

Results & Discussion

4.1 Results

Fig. 1 shows how γ affects J_{0D}, derived from both the diffusive model and the QSS model, with $\beta = 1000$. When $\gamma = 0$, both numerical solutions match exactly with the associated analytical solutions given in Eqs. (3.18) and (3.20). When $\gamma = 10^5$, both numerical solutions match exactly with the associated analytical solutions given in Eqs. (3.19) and (3.21) (which were derived assuming $\gamma \to \infty$). For an intermediate γ value of 10, the results are situated in between the two end member solutions.

The absolute dimensionless error between J_{0D} and J^*_{0D} for different values of γ, when $\beta = 1000$, is presented in Fig. 2. Again it can be seen that the error responses for intermediate values of γ are situated between the two end member solutions for $\gamma \to \infty$ and $\gamma \to 0$. Also shown as circular markers, are the evaluated dimensionless diffusion equilibrium times, τ_{cr}, as previously defined in Section 3.5. It can be seen that τ_{cr} decreases with increasing γ. It is also apparent that $1 \leq \tau_{cr} \leq 1 + \beta$.

The analysis presented in Fig. 2 was repeated for a range of different β values and a range of different γ values. As β is increased, the error response looks similar but is drawn out over progressively longer periods of time. Values of τ_{cr} were collected for each of the simulations undertaken, which are presented collectively in Fig. 3.

The results in Fig. 3 shows plots of $(\tau_{cr} - 1)/\beta$ on the y-axis to normalise all

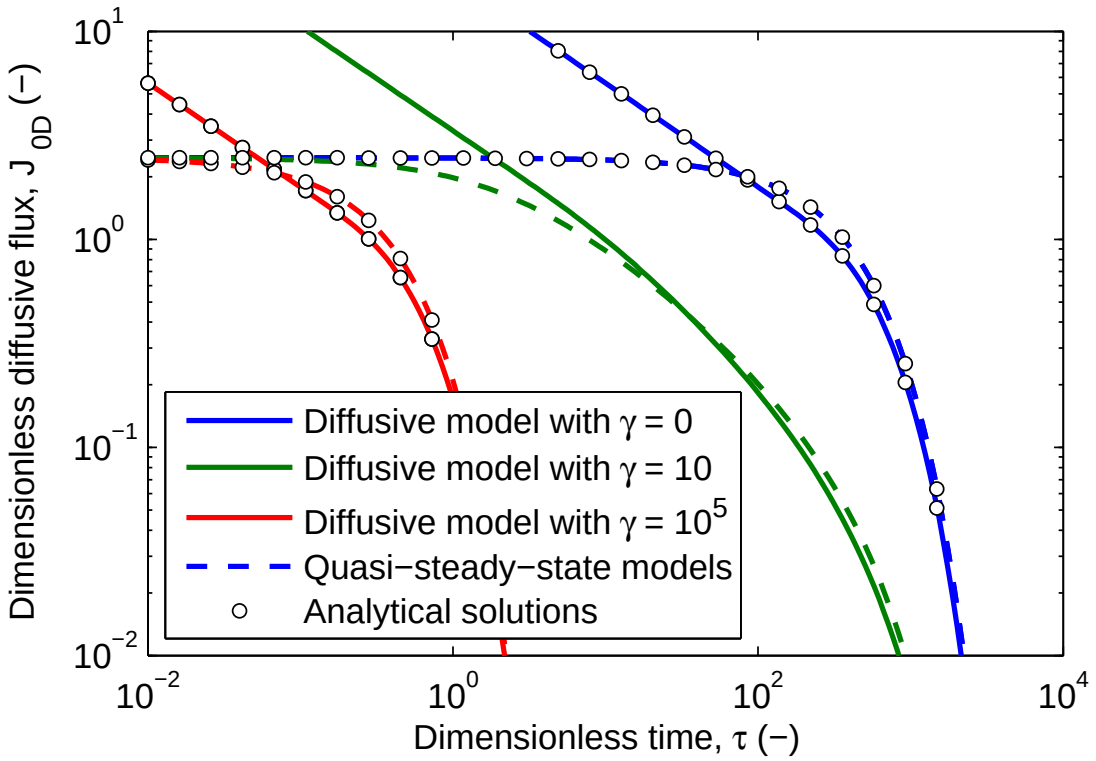

Figure 4.1: Plots of dimensionless diffusive flux, J_{0D}, against dimensionless time, τ, with $\beta = 1000$ and γ values as indicated in the legend. The solid lines are results from the finite difference model for the full diffusion problem. The dashed lines are from the numerical solution of the quasi-steady-state model. The circular markers are from the analytical solutions given in Eqs. (3.18) to (3.21). Note that the analytical solutions used for the $\gamma = 10^5$ scenario involved assuming $\gamma \to \infty$.

the model results between zero and one. It is apparent that the relationship between $(\tau_{cr} - 1)/\beta$ and γ is largely independent of β. A heuristic function, $\exp(-\gamma/2)$, was found, by trial and error, to approximate a significant part of the analysis. It follows, given Eq. (3.10), that an estimate of the diffusion equilibrium time for non-zero a scenarios can be found from

$$t_{cr} = \frac{L^2}{4D_E}\left[\phi + \rho_b b \exp\left(-\frac{ac_I}{2}\right)\right] \tag{4.1}$$

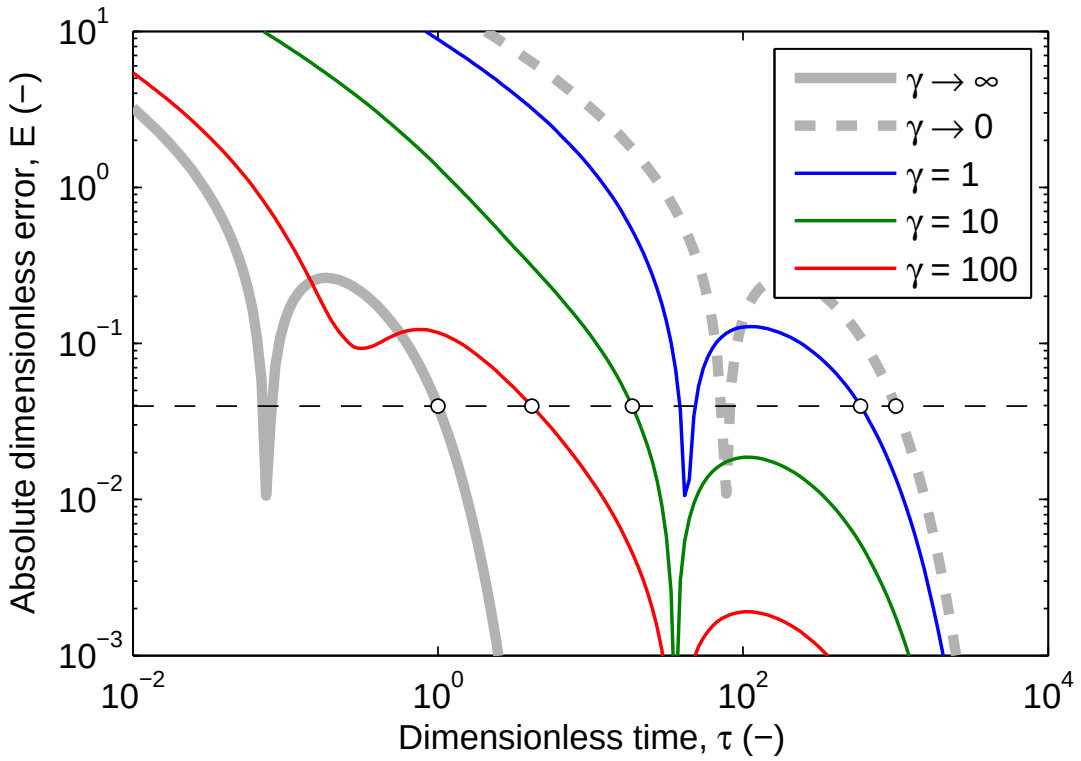

Figure 4.2: Plots of absolute dimensionless error between the diffusive fluxes calculated using the diffusive model and the quasi-steady-state model (this is calculated using Eq. (3.22)) with $\beta = 1000$ and γ as indicated in the legend. The horizontal black dashed line indicates the value of error at which the diffusion equilibrium time is thought to have been reached (i.e., $E = 0.03964$). The circular markers indicate the evaluated dimensionless diffusion equilibrium times, τ_{cr}, for each of the model scenarios presented.

4.1.1 Application to shale gas systems

Two case studies based on shale reservoirs described in Etminan et al. (2014) (Case 1) and Weniger et al. (2010) (Case 2) are presented. The relevant reservoir parameters for each case study are presented in Table A.1. Where necessary, units have been converted to SI from the literature values. For Case 1, a representative diffusion coefficient is taken from Li and Meng (2016) and fracture spacings estimated from Lash and Engelder (2005). For Case 2, porosity and bulk volume are also assumed values.

Eq. (4.1) then permits estimation of the relevant DETs for each shale case as presented in Table 4.1.

It is noted that these two contrasting shale gas case studies both produce estimated DETs that indicate the quasi-steady state approximation would be an appropriate as-

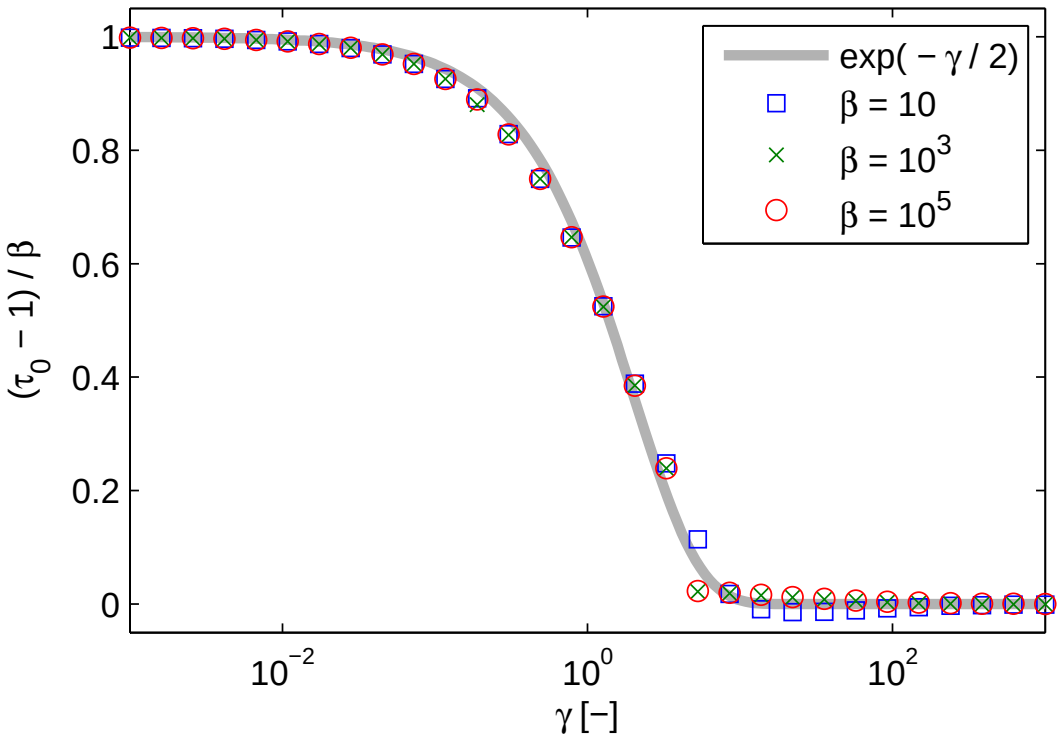

Figure 4.3: Plot of evaluated dimensionless diffusion equilibrium times, τ_{cr}, against γ for different values of β as indicated in the legend. The thick grey line shows results from a heuristic function proposed to represent the main features of the observed model response.

	Case 1	Case 2	Unit
DET	1.59	1.25	s

Table 4.1: Calculated diffusion equilibrium times - shale cases

sumption in modelling these systems, since the period of interest in terms of production is very substantially longer that the calculated DETs.

4.1.2 Application to coalbed methane systems

Two further case studies based on CBM reservoirs described in Zarrouk and Moore (2009) (Case 3 - low rank coal) and Cui and Bustin (2005) (Case 4 - high rank coal) are presented. The relevant reservoir parameters for each case study are presented in Table B.1. Where necessary, units have been converted to SI from literature values. The diffusion coefficient for Case 3 has been taken from Xu et al. (2015) as a representative

	Case 3	Case 4	Unit
DET	6.2E3	1.87E5	s

Table 4.2: Calculated diffusion equilibrium times - coalbed methane cases

value for a low rank coal at 4 MPa. Bulk density for Case 3 comes from Crosdale et al. (2008). For Case 4, cleat spacing, porosity and reservoir pressure are assumed values.

Eq. (4.1) then permits estimation of the relevant DETs for each CBM case as provided in Table 4.2. For Case 3, the DET is estimated at under 2 minutes and for Case 4, the DET is approximately 52 hours.

In contrast to the shale case studies, the coalbed methane cases suggest a much broader range of diffusion equilibrium times may be present in coal. While the DET for the low rank coal suggests the QSS approximation would be valid for production modelling, the calculated DET for the high rank coal is significantly larger. In terms of production modelling, it may still be appropriate to employ the QSS assumption for both cases, since the timescale of interest in production is much longer than the calculated 52 hours. However, greater caution may be recommended in coal cases and each case should be evaluated individually, prior to invoking the QSS model.

Chapter 5

Conclusions & Recommendations

5.1 Conclusions

This study has explored DETs for gas diffusion with Langmuir isotherm adsorption by numerical solution. A heuristic function has been derived, which permits rapid estimation of DET for diffusive systems with associated Langmuir isotherm adsorption. Understanding of the DET for individual systems permits appropriate application of the QSS assumption, with the associated benefits of computational efficiency. It also highlights those cases where further investigation may be required or where a more suitable representation, such as a fully diffusive model, must be employed.

The case studies presented indicate the QSS model may be suited to both shale gas and CBM production scenarios, since DETs in these systems have been found to be suitably short, relative to the timescales of interest for production.

It is noted, however, that given the variety and uncertainty present in shale and CBM reservoirs that cases should be evaluated individually prior to applying the QSS model.

5.2 Recommendations for further work

Further work to fit the proposed model to experimental desorption data would enhance the validity of the approach. Direct comparison to other commonly used methods, such as the model developed by (King et al., 1986) which permits diffusion only within the matrix and desorption only at the cleat/fracture surface, may provide further insight to diffusion processes in shale and coal. King's (1986) model benefits from permitting application of analytical solutions to certain cases. However, fitting the analytical solutions to desorption datasets is often problematic. Authors have sought to resolve these difficulties by invoking time-dependent diffusion coefficients (Yue et al., 2017; Dong et al., 2017). However, such an approach does not enhance insight into the physical processes occurring within the system. Variation in diffusion coefficient observed during a diffusion experiment is more likely linked to physical changes within the system, rather than any innate time-dependence of the diffusion coefficient. The model proposed in this study may address some of these concerns.

Work to demonstrate field-scale application of the modelling approach would demonstrate the utility of the proposed model.

Work to incorporate the heterogeneity observed in shale and CBM systems could give further insight into factors influencing gas production from such reservoirs. Within this, incorporation of pressure-dependent fracture permeability could permit some enhanced understanding of the relevance of unpropped fractures to gas production. However, it remains important to recognise the degree of uncertainty present in the characterisation of many shale and CBM reservoirs. Detailed numerical analysis of individual reservoirs may not be feasible, where the related models are reliant on uncertain input data or significant assumptions. To this end, ongoing work to reduce uncertainties will be useful to future modelling efforts.

References

Allan, A. M. and Mavko, G. (2013). "The effect of adsorption and Knudsen diffusion on the steady-state permeability of microporous rocks." *Geophys.*, 78(2), D75–D83.

Ambrose, R. J., Hartman, R. C., and Akkutlu, I. Y. (2011). "Multi-component sorbed phase considerations for shale gas-in-place calculations." *SPE Production and Operations Symposium*, Society of Petroleum Engineers, Oklahoma City, 27–29 March. SPE 141416.

Ambrose, R. J., Hartman, R. C., Campos, M. D., Akkutlu, I. Y., and Sondergeld, C. (2010). "New pore-scale considerations for shale gas-in-place calculations." *SPE Production and Operations Symposium*, Society of Petroleum Engineers, Pittsburgh, 23–25 February. SPE 131772.

Barenblatt, G. I., Zheltov, I. P., and Kochina, I. N. (1960). "Basic concepts in the theory of seepage of homogeneous liquids in fissured rocks [strata]." *J. Appl. Math. Mech.*, 24(5), 852–864.

Barker, J. A. (1991). "Transport in fractured rocks." *Applied Groundwater Hydrology*, R. A. Downing and W. B. Wilkinson, eds., Clarendon Press, Oxford, chapter 13.

Bello, R. O. and Wattenbarger, R. A. (2010). "Modelling and analysis of shale gas production with a skin effect." *JCPT*, 49(12), 37–48.

Bumb, A. C. and McKee, C. R. (1988). "Gas-well testing in the presence of desorption for coalbed methane and Devonian shale." *SPE Formation Evaluation*, 3(01), SPE 15277.

Cheng, Y. (2011). "Pressure transient characteristics of hydraulically fractured horizontal shale gas wells." *SPE Eastern Regional Meeting*, Society of Petroleum Engineers, Columbus, 17-19 August. SPE 149311.

Cipolla, C. L., Lolon, E. P., Erdle, J. C., and Rubin, B. (2010). "Reservoir modeling in shale-gas reservoirs." *SPE Reservoir Evaluation and Engineering*, 13(04), SPE 125530.

Crosdale, P. J., Beamish, B. B., and Valix, M. (1998). "Coalbed methane sorption related to coal composition." *Int. J. Coal Geol.*, 35, 147–158.

Crosdale, P. J., Moore, T. A., and Mares, T. E. (2008). "Influence of moisture content and temperature on methane adsorption isotherm analysis for coals from a low-rank, biogenically-sourced gas reservoir." *Int. J. Coal Geol.*, 76, 166–174.

Cui, X. and Bustin, R. M. (2005). "Volumetric strain associated with methane

desorption and its impact on coalbed gas production from deep coal seams." *AAPG Bull.*, 89, 1182–1202.

Curtis, J. B. (2002). "Fractured shale-gas systems." *AAPG Bull.*, 86(11), 1921–1938.

Curtis, M. E., Cardott, B. J., Sondergeld, C. H., and Rai, C. S. (2011). "Investigation of the relationship between organic porosity and thermal maturity in the marcellus shale." *North American Unconventional Gas Conference and Exhibition*, Society of Petroleum Engineers, The Woodlands, 14–16 June. SPE 144370.

Curtis, M. E., Cardott, B. J., Sondergeld, C. H., and Rai, C. S. (2012). "Development of organic porosity in the Woodford shale with increasing thermal maturity." *Int. J. Coal Geol.*, 103(4), 26–31.

Ding, D. Y., Wu, Y.-S., Farah, N., Wang, C., and Bourbiaux, B. (2014). "Numerical simulation of low permeability unconventional gas reservoirs." *SPE/EAGE European Unconventional Resources and Exhibition, Session 11: Economic Risk and Reserves 1*, Society of Petroleum Engineers, Vienna, 25-27 February. SPE 167711.

Dong, J., Cheng, Y., Liu, Q., Zhang, H., Zhang, K., and Hu, B. (2017). "Apparent and true diffusion coefficients of methane in coal and their relationships with methane desorption capacity." *Energy & Fuels*.

Etminan, S. R., Javadpour, F., Maini, B. B., and Chen, Z. (2014). "Measurement of gas storage processes in shale and of the molecular diffusion coefficient in kerogen." *Int. J. Coal Geol.*, 123, 10–19.

Foo, K. Y. and Hameed, B. H. (2010). "Insights into the modelling of adsorption isotherm systems." *Chem. Eng. J.*, 156, 2–10.

Freeman, C. M., Moridis, G., Ilk, D., and Blasingame, T. A. (2013). "A numerical study of performance for tight gas and shale gas." *J. Petrol. Sci. Eng.*, 108(August), 22–39.

Gao, C., Lee, W. J., Spivey, J. P., Semmelbeck, M. E., and Holditch, S. A. (1994). "Modeling multilayer gas reservoirs including sorption effects." *SPE Eastern Regional Conference and Exhibition*, Society of Petroleum Engineers, Charleston, 8–10 November. SPR 12173.

Hildenbrand, A., Krooss, B. M., Busch, A., and Gaschnitz, R. (2006). "Evolution of methane sorption capacity of coal seams as a function of burial history - a case study from the Campine Basin, NE Belgium." *Int. J. Coal Geol.*, 66, 179–203.

Hill, D. G. and Nelson, C. R. (2000). "Gas productive fractured shales: an overview and update." *Gas Tips*, 6(3), 4–13.

Hu, H. (2014). "Methane adsorption comparison of different thermal maturity kerogens in shale gas system." *Chinese J. Geochem.*, 33(4), 425–430.

King, R. K., Ertekin, T., and Scwerer, F. C. (1986). "Numerical simulation of the transient behavior of coal-seam degasification wells." *SPE Form. Eval.*, April.

Krooss, B. M., van Bergen, F., Gensterblum, Y., and Siemons, N. (2002). "High-

pressure methane and carbon dioxide adsorption on dry and moisture-equilibrated Pennsylvanian coals." *Int. J. Coal Geol.*, 51, 69–92.

Kuila, U. and Prasad, M. (2011). "Surface area and pore-size distribution in clays and shales." *SPE Annual Technical Conference and Exhibition*, Society of Petroleum Engineers, Denver, 30 October – 2 November. SPE 146869.

Lash, G. G. and Engelder, T. (2005). "An analysis of horizontal microcracking during catagenesis: Example from the catskill delta complex." *AAPG Bull.*, 89, 1433–1449.

Leahy-Dios, A., Das, M., Agarwal, A., and Kaminsky, R. D. (2011). "Modelling of transport phenomena and multicomponent sorption for shale gas and coalbed methane in an unstructured grid simulator." *SPE Annual Technical Conference and Exhibition*, Society of Petroleum Engineers, Denver, 30 October–2 November. SPE 147352.

Li, G. and Meng, Z. (2016). "A preliminary investigation of ch 4 diffusion through gas shale in the paleozoic longmaxi formation, southern sichuan basin, china." *J. Nat. Gas Sci. Eng.*, 36, 1220–1227.

Loucks, R., Reed, R., Ruppel, S. C., and Hammes, U. (2012). "Spectrum of pore types and networks in mudrocks and a descriptive classification for matrix-related mudrock pores." *AAPG Bull.*, 6, 1071–1098.

Mathias, S. A., Butler, A. P., and Zhan, H. (2008). "Approximate solutions for forchheimer flow to a well." *J. Hydraulic Eng.*, 134, 1318–1325.

Mathias, S. A. and Zimmerman, R. W. (2003). "Laplace transform inversion for late-time behavior of groundwater flow problems." *Water Res. Res.*, 39, 1283.

Medved, I. and Cerny, R. (2011). "Surface diffusion in porous media." *Mic. Mes. Mat.*, 142(2–3), 405–422.

Moridis, G. J., Blasingame, T. A., and M, F. C. (2010). "Analysis of mechanisms of flow in fractured tight-gas and shale-gas reservoirs." *SPE Latin American and Caribbean Petroleum Engineering Conference*, Society of Petroleum Engineers, Lima, 1–3 December. SPE 139250.

Pillalamarry, M., Harpalani, S., and Liu, S. (2011). "Gas diffusion behavior of coal and its impact on production from coalbed methane reservoirs." *Int. J. Coal Geol.*, 86, 342–348.

Rickman, R., Mullen, M., Petre, E., Grieser, B., and Kundert, D. (2008). "A practical use of shale petrophysics for stimulation design optimization: all shale plays are not clones of the barnett shale." *SPE Annual Technical Conference and Exhibition*, Society of Petroleum Engineers, Denver, 21–24 September. SPE 115258.

Sakhaee-Pour, A. and Bryant, S. L. (2011). "Gas permeability of shale." *SPE Reservoir Evaluation and Engineering*, 15(04), SPE 146944.

Shi, J. Q. and Durucan, S. (2008). "Modeling of mixed-gas adsorption and diffusion in coalbed methane reservoirs." *SPE Unconventional Reservoirs Conference*, Society of Petroleum Engineers, Keystone, 10–12 February. SPE 114197.

Sinha, S., Braun, E., Determan, M., Passey, Q., Leonardi, S., Boros, J., Wood III, A., Zirkle, T., Kudva, R., et al. (2013). "Steady-state permeability measurements on intact shale samples at reservoir conditions-effect of stress, temperature, pressure, and type of gas." *SPE Middle East Oil and Gas Show and Conference*, Society of Petroleum Engineers, Manama, 10–13 March. SPE 164263.

Sondergeld, C. H., Newsham, K. E., Comisky, J. T., Rice, M. C., and S, R. C. (2010). "Petrophysical considerations in evaluating and producing shale gas." *SPE Unconventional Gas Conference*, Pittsburgh, 23–25 February. SPE 131768.

Su, Y., Zhang, Q., Wang, W., and Sheng, G. (2015). "Performance analysis of a composite dual-porosity model in multi-scale fractured shale reservoir." *J. Nat. Gas Sci. Eng.*, 26(September), 1107–1118.

Tang, X., Ripepi, N., Luxbacher, K., and Pitcher, E. (2017). "Adsorption models for methane in shales: Review, comparison, and application." *Energy & Fuels*, 0(0), null.

Thimmons, E. D. and Kissell, F. N. (1973). "Diffusion of methane through coal." *Fuel*, 52(4), 274–280.

U.S.E.I.A (2018). *U.S. Crude Oil and Natural Gas Proved Reserves, Year End 2016*. U.S. Department of Energy, Washington.

Weniger, P., Kalkreuth, W., Busch, A., and Krooss, B. M. (2010). "High-pressure methane and carbon dioxide sorption on coal and shale samples from the parana basin, brazil." *Int. J Coal Geol.*, 84, 190–205.

Xu, H., Tang, D., Zhao, J., Li, S., and Tao, S. (2015). "A new laboratory method for accurate measurement of the methane diffusion coefficient and its influencing factors in the coal matrix." *Fuel*, 158(October), 239–247.

Yang, R. T. (1997). *Gas Separation by Adsorption Processes*. Imperial College Press, London.

Yang, Y. and Aplin, A. C. (2007). "Permeability and petrophysical properties of 30 natural mudstones." *J. Geophys. Res. - Sol. Ea.*, 112(B3).

Yue, G., Wang, Z., Xie, C., Tang, X., and Yuan, J. (2017). "Time-dependent methane diffusion behavior in coal: measurement and modeling." *Transp. Porous Media*, 116, 319–333.

Zarrouk, S. J. and Moore, T. A. (2009). "Preliminary reservoir model of enhanced coalbed methane (ecbm) in a subbituminous coal seam, huntly coalfield, new zealand." *Int. J. Coal Geol.*, 77, 153–161.

Zhang, T., Ellis, G., Ruppel, S. C., Milliken, K., and Yang, R. (2012). "Effect

of organic-matter type and thermal maturity on methane adsorption in shale-gas systems." *Org. Geochem.*, 47(June), 120–131.

Appendix A

Case study parameters - shale

Parameter	Case 1	Case 2	Unit
L	2E-5	2E-5	m
D_E	8E-12	1.3E-11	m^2
ϕ	0.08	0.05	(-)
ρ_b	2589	2330	kg m^{-3}
s_{max}	0.0015	0.0029	kg kg^{-1}
b	4.13E-5	8.28E-5	m^3 kg^{-1}
a	2.75E-2	2.85E-2	m^3 kg^{-1}
c_i	59.6	37.8	kg m^{-3}
T_{res}	323	318	K

Table A.1: Case study parameters - shale

Appendix B

Case study parameters - coal

Parameter	Case 3	Case 4	Unit
L	0.02	0.008	m
D_E	6E-10	1E-11	m^2
ϕ	0.02	0.025	(-)
ρ_b	1300	1450	kg m^{-3}
s_{max}	0.4631	7.4517	kg kg^{-1}
b	1.02E-2	2.11E-1	m^3 kg^{-1}
a	2.19E-2	2.84E-2	m^3 kg^{-1}
c_i	24.6	122	kg m^{-3}
T_{res}	313	393	K

Table B.1: Case study parameters - CBM